Developing empirical relationships to estimate porosity and microhardness of plasma-sprayed YSZ coatings

S. Karthikeyan[a,1], V. Balasubramanian[b,*], R. Rajendran[c,2]

[a]Department of Manufacturing Engineering, Annamalai University, Annamalai Nagar 608 002, India
[b]Centre for Materials Joining and Research (CEMAJOR), Department of Manufacturing Engineering, Annamalai University,
Annamalai Nagar (P.O.) 608 002, India
[c]Materials Technology Group, Gas Turbine Research Establishment (GTRE), Bengaluru 560 093, India

Abstract

Plasma-sprayed yttria-stabilized zirconia (YSZ) coating has been considered to be a good protective coating material for high-temperature applications on account of its superior properties and life cycle costs. However, thermal barrier coatings (TBCs) have engineering reliability problems in tailoring the microstructure and mechanical properties towards achieving both prime reliance and manufacturing reproducibility. In this work, empirical relationships were developed to estimate TBCs performance characteristics (porosity and microhardness) by incorporating independently controllable atmospheric plasma spray operational parameters (input power, standoff distance and powder feed rate) using the response surface methodology (RSM). A central composite rotatable design with three factors and five levels was chosen to minimize the number of experimental conditions. Within the scope of the design space, the input power and the standoff distance appeared to be the most significant two parameters affecting the coating quality characteristics among the three investigated process parameters. Further, correlating the spray parameters with coating properties enables the identification of characteristics regime to achieve desired quality of YSZ coatings.
© 2013 Elsevier Ltd and Techna Group S.r.l. All rights reserved.

Keywords: B. Porosity; C. Hardness; D. ZrO$_2$; E. Thermal applications

1. Introduction

Thermal barrier coatings (TBCs) protect the hot-section stationary and rotating components of gas turbines [1,2]. Generally, TBC systems are deposited by atmospheric plasma spray (APS) and electron beam physical vapor deposition (EB-PVD) processes. APS is the more commercial method, because of less expensive and lower thermal conductivity than EB-PVD, even though there are many defects such as pores, microcracks and unmelted particles, showing a lower strain tolerance than EB-PVD [3–5]. Plasma-sprayed yttria partially stabilized

zirconia (YSZ) coatings are among the most widely used protective coating materials in aerospace and power generation gas turbines [6]. APS is a versatile thermal spray process; however, melting of feedstock particles, flattening and solidification of plasma-sprayed particles impinging on a substrate surface are very complex phenomena involving rapid changes in the dynamic and thermal state of the molten particles that depend on many factors [7]. It is difficult to setup the process control due to the involvement of many process parameters in APS as the evolution of the complex microstructure of plasma-sprayed coatings is related to a number of processing variables. The establishment of a rigorous relationship between spray parameters and structure of a coating is the key point which will lead to production of a desirable coating. The thermo-mechanical properties of plasma-sprayed thermal barrier coatings are very strongly dependent on the microstructure, and this may be controlled by manipulating the parameters controlling the plasma spray process [8].

*Corresponding author. Tel.: +91 4144 239734, mobile: +91 9443412249; fax: +91 4144 239734/238 275.

E-mail addresses: azhagarkarthi@gmail.com (S. Karthikeyan),
visvabalu@yahoo.com, balasubramanian.v.2784@annamalaiuniversity.ac.edu
(V. Balasubramanian), rajendran@gtre.drdo.in (R. Rajendran).
[1]Tel.: +91 9843856891.
[2]Tel.: +91 80 25040169; fax: +91 80 25241507.

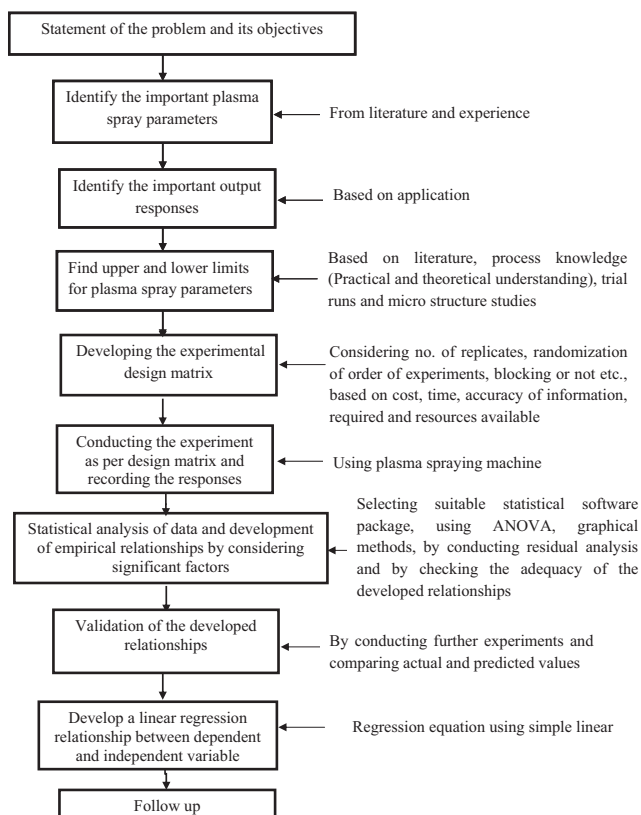|	
Statement of the problem and its objectives	
Identify the important plasma spray parameters	From literature and experience
Identify the important output responses	Based on application
Find upper and lower limits for plasma spray parameters	Based on literature, process knowledge (Practical and theoretical understanding), trial runs and micro structure studies
Developing the experimental design matrix	Considering no. of replicates, randomization of order of experiments, blocking or not etc., based on cost, time, accuracy of information, required and resources available
Conducting the experiment as per design matrix and recording the responses	Using plasma spraying machine
Statistical analysis of data and development of empirical relationships by considering significant factors	Selecting suitable statistical software package, using ANOVA, graphical methods, by conducting residual analysis and by checking the adequacy of the developed relationships
Validation of the developed relationships	By conducting further experiments and comparing actual and predicted values
Develop a linear regression relationship between dependent and independent variable	Regression equation using simple linear
Follow up	

Fig. 1. Flow chart for scheme of investigation.

Coating properties like porosity, Young's modulus, phase composition, and coating residual stresses determine to a large extent the performance of TBC during service [9]. The porosity is usually used as a parameter of the structure of plasma-sprayed coating [10]. The pores and cracks interfere with the direct flow of heat (thermal barrier) resulting in lowered thermal conductivity. Furthermore, the porosity, cracks and myriad array of interfaces also offer mechanical compliance to this system enabling their thermo-mechanical compatibility during cyclic thermal exposure between room temperature and over 1000 °C operating temperature [11,12].

As for all materials, the hardness of a coating is a measure of the resistance to plastic deformation. It is widely recognized that the hardness increases with the increasing coating density, i.e. decreasing number of pores and microcracks [13]. Although the porosity of the present TBCs is low, the flexibility is expected to be high owing to the deliberate formation of a dense network of microcracks.

Conventional methods for studying the effect of some parameters on a process are performed by varying one parameter at a time, maintaining all the other parameters constant, and fixing the best value achieved for each parameter. The disadvantage of this univariate procedure is that the best conditions could not be attained because the interaction effects between the parameters are discarded. Moreover, conventional methods are time-consuming and require a large number of experiments to determine the optimum conditions of a process. These drawbacks of conventional methods can be eliminated by studying the effect of operational parameters such as input power, standoff distance and powder feed rate using design of experiments, which allow the measurement of the main effects of each parameter and the interaction effects between parameters [14,15]. It has been proved by several researchers [16–19] that efficient use of statistical design of experimental techniques allows the development of an empirical methodology to incorporate a scientific approach in the plasma spraying procedure.

Researchers across the globe tried to model thermal spraying processes using statistical regression techniques. Mawdsley et al. [20] carried out statistically designed experiments and multiple regression analysis to identify the effects of process parameters on the three properties of plasma-sprayed alumina coatings, namely permeability, hardness and thickness. The parameters, viz., powder injection angle, powder injection offset, plasma gun power, plasma gas flow, percent of hydrogen in plasma gas flow and spray distance, had been used in a 2-level fractional factorial design of experiments; and the parameters, namely carrier gas flow, spray distance, power and plasma gas flow, had been considered in a 3-level D-optimal design of experiments. A uniform design method was utilized by Li et al. [21] to analyze the dependence of deposition efficiency, porosity, oxide content, microhardness and fracture toughness on process parameters of plasma-sprayed TiN coatings. Again, Li et al. [22] used a uniform design of experiments for optimizing the plasma spray process parameters of yttria-stabilized zirconia coatings. The third-order regression equations obtained from their analysis were the most appropriate ones to identify the influence of process parameters. A D-optimal experimental design had been used by Azarmi et al. [23] to characterize the effects of atmospheric plasma spray process parameters on inflight particle temperature and velocity, and on the oxide content and porosity in a nickel-based super-alloy coating. Recently, A 2^4 factorial design of experiments was utilized by Forghani and his associates [24] to analyze the correlation between the process variables on important properties of the coatings such as microhardness, thickness/cycle, deposition efficiency and porosity.

Although extensive research has been performed to model this process, the reported research work on relating the operational plasma spray parameters and coating characteristics is very scanty. Moreover, only very few investigations have been carried out to estimate the porosity and the microhardness of TBCs incorporating plasma spray parameters. Hence, in this investigation, an attempt was made to develop empirical relationships to estimate the porosity and microhardness of plasma-sprayed YSZ coatings using statistical tools such as design of experiments, analysis of variance and regression analysis.

2. Scheme of investigation

In order to achieve the desired objectives, this present investigation was planned as depicted in the flow chart (Fig. 1).

Table 1
Chemical composition (wt%) of substrate material (C263).

Co	Cr	Mn	Mo	Fe	Ti	Al	Zr	Si	Ni
19.32	19.87	0.431	5.858	0.011	1.956	0.403	0.137	0.22	Bal

2.1. Identifying the important process parameters

An initial step in the design of experiments is to select independently controllable process parameters. It has been widely recognized in the thermal spray community that there are many hundreds of parameters, which can potentially influence the properties of the coatings. For economic (time requirements) and theoretical reasons (interdependence of parameters), it is not possible to control all possible parameter variations. From the literature [25–27] and the previous work done [28,29] in our laboratory, the predominant factors which are having more influence on coating characteristic in plasma spraying process were identified. They are as follows:

(i) Input power (kW).
(ii) Primary gas flow rate (lpm).
(iii) Standoff distance (mm).
(iv) Powder feed rate (mm).
(v) Carrier gas flow rate (lpm).

These are the primary operational parameters contributing to the melting and flattening of the powder particles, subsequently, influencing the coating characteristics of plasma-sprayed YSZ coatings.

2.2. Finding the working limits of the parameters

A large number of spraying trials were conducted on grit-blasted 2-mm-thick C263 nickel-based super alloy substrate coupons to determine the feasible working range of the above factors by varying one of the APS spray parameters and keeping the rest of them at constant value. The chemical composition of the polycrystalline super alloy, Superni C263 substrate material used in this investigation, was found by the optical emission spectroscopy method and is presented in Table 1. The feedstock was spray-dried and densified Zirconia–Yttria 8% stabilized powder (Powder Alloy corporation, USA, PAC 2008P) with a particle size of $-106+15$ µm. The SEM image (Model: JEOL 6410-LV) of the feedstock taken at $200\times$ magnification with an image resolution of 1024×768 pixels shows spherical morphology, some particles having satellites as shown in Fig. 2. Plasma spray deposition was carried out using an APS system 40 kW IGBT-based Plasmatron (Make: Ion Arc Technologies; India. Model: APSS-II). The YSZ powder was directly sprayed on to the grit-blasted substrate to a thickness of 300 ± 10 µm and a bond coat was not used [5,22,28]. The cracks and delamination of the coating, the thickness developed per pass, and avoiding markedly seeing open pores by naked eye were inspected to identify
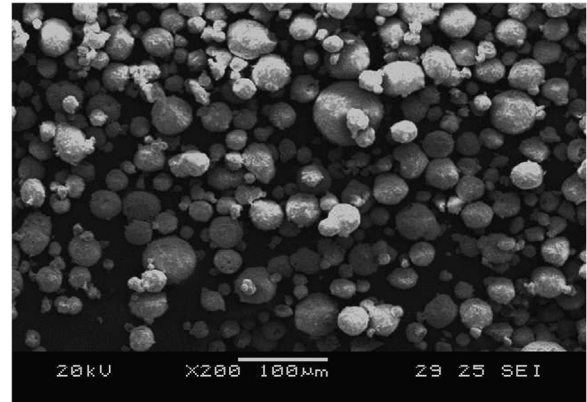

Fig. 2. SEM image of 8YSZ powder.

the working limits of the operational plasma spray parameters, leading to the following observations and also seen in Fig. 3.

(1) If the input power was less than 20 kW, the poor melting of powders and unmelted powder particles deposited on the substrate surface were observed (Fig. 3a). For the input power greater than 28 kW, over heating of the substrate, the formation of quench cracks and splashing were noticed during spraying (Fig. 3b). Under higher power levels, stresses can be generated within the coating owing to the contraction of individual sprayed splats during rapid cooling (10^6–10^8 K/s) and resolidification on the colder substrate or on a layer of previously solidified splats. This generated stresses are called as 'quenching stresses' [30,31]. These stresses were relieved by forming cracks in the coating due to the higher heating rate of splats.

(2) In order to provide sufficient enthalpy to the injected powder particles, keeping the plasma column length in an acceptable range to increase the particles residential time in the jet, the primary gas flow rate was kept in a constant level of 35 lpm. Under this condition, there exists an optimum plume position where the maximum energy transfer from plasma to particle is accomplished for ceramics [32,33]. In this study, argon gas was used as a plasma forming gas. This effect was clearly described in the published literatures [28,34].

(3) If the standoff distance was less than 100 mm, there was an over deposition of coating and also substrate deformation with delamination was observed (Fig. 3c). Standoff distance greater than 130 mm resulted in resolidification of particles and molten particles not reaching the target, this resulted in poor deposition rate (Fig. 3d).

(4) Due to the limitation of the powder feeding system in the present experimental setup, the minimum possible powder feed rate was achieved as 18 gpm. If the powder feed rate was increased beyond 38 gpm, resulting in clogging of powder particles in the powder injection port.

(5) If the carrier gas flow rate was below 5 lpm, then the powder port turned in to red hot condition, and if it was increased beyond 7 lpm, then the powder particles fly away from the plasma column and also arc blow out was observed. Nitrogen was used as a secondary gas, and its flow rate was kept constant at 3 lpm.
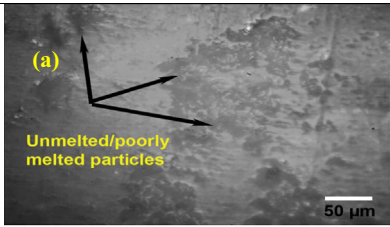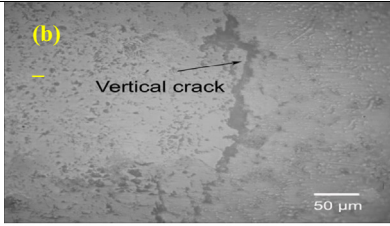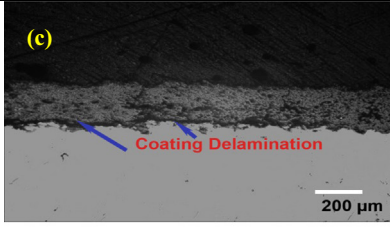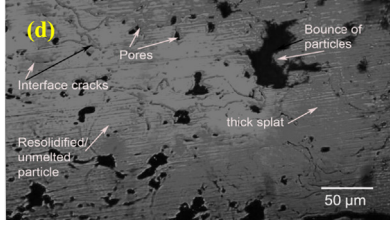
Parameter	Level	Microstructural Features	Observations
power	< 20 kW		Poor melting, unmelted particles present in the coating matrix
Power	> 28 kW		Resulted in quench cracks
Standoff distance	<100 mm		Coating delamination
Standoff distance	> 130 mm		Resoldification of molten particles and more interfacial cracks

Fig. 3. Microstructural observations during plasma-sprayed yttria-stabilized zirconia coating trials.

It is very hard to set up the process control due to the involvement of many process parameters in APS. There is an associated cost to optimize the plasma spray parameters for new coating materials. Therefore, there is a need to reduce the variables in manageable numbers. The molten powder particles flattening and splat formation are sensitive to the processing parameters, especially to the input power, standoff distance and the powder feed rate. Primary gas flow rate was kept in a constant level of 35 lpm to provide sufficient enthalpy to the powder particles. To get an optimum penetration of the powder particles in the plasma column, the carrier gas flow rate also was standardized into 7 lpm. Hence, in this investigation, the chosen spray parameters were viz power, standoff distance and powder feed rate because these parameters are directly measured and easier to control in real-time.

2.3. Developing the experimental design matrix

By considering all the above conditions, the feasible limits of the parameters were chosen in such a way that plasma spray deposition was carried out to deposit coatings without defects on the substrate. Central composite rotatable design of second order was found to be the most efficient tool in the response surface methodology to establish the mathematical relation of the response surface using the smallest possible number of experiments without losing its accuracy [35]. Due to wide range of factors, it was decided to use three factors, five levels and central composite design matrix to develop a mathematical model for the experimental conditions. Central composite design is the most popular response surface method design, which has three groups of design points such as factorial points, axial or star points and center points. The factorial part of the design consists of all possible combinations of the upper (+1) and the lower levels (−1) of the factors. The star points have all the factors set to 0, the midpoint, except one factor, which has the value +/− Alpha (+/− 1.682) for both rotatability and orthogonality of blocks. Center points, as implied by the name, are points with all levels set to coded level 0 − the midpoint of each factor range. The center points (in this investigation, 15 − 20) are usually repeated 4 − 6 times to get a good estimate of the experimental error (pure error). To summarize, central composite designs require 5 levels of

each factor: $-$Alpha, -1, 0, 1, and $+$Alpha. One of the commendable attributes of the central composite design is that its structure lends itself to sequential experimentation [36]. Table 2 presents the ranges of factors considered and Table 3 shows the 20 sets of coded conditions used to form the design matrix. The first eight experimental conditions are derived from factorial experimental design matrix ($2^3 = 8$). All the variables at the intermediate (0) level constitute the center points while the combinations of each process variable at either its lowest (-1.682) or its highest ($+1.682$) with the other six variables of the intermediate levels constitute the star points. Thus, the 20 experimental conditions allowed the estimation of the linear, quadratic and two-way interactive effects of the variables on the porosity and microhardness of plasma-sprayed YSZ coatings. The method of designing such a matrix is dealt with elsewhere [37,38].

For the convenience of recording and processing of the experimental data, upper and lower levels of the factors are coded as $+1.682$ and -1.682, respectively. The following relationship can be effectively used to calculate any

intermediate levels in the coded form:

$$X_i = 1.682[2X - (X_{max} + X_{min})]/[X_{max} - X_{min}] \qquad (1)$$

where X_i is the required coded value of a variable X, X is any value of the variable from X_{min} to X_{max}, X_{min} is the lower level of the variable, and X_{max} is the highest level of the variable.

2.4. Conducting the experiments and recording the responses

2.4.1. Plasma spray deposition

In this present investigation, the plasma spraying was carried out according to the design of experiments; at each condition, three specimens were coated as prescribed by the design matrix. The experiments were conducted in a random order to prevent systematic errors infiltrating the system. To evaluate the coating properties, substrates with the dimensions of 25.4×12.7 mm were used for metallographic examination and microhardness measurement. The substrates were prepared by grit blasting before the deposition of the coating. Grit blasting was carried out using corundum grits of size of 500 ± 320 µm and subsequently cleaned using acetone in an ultrasonic bath and dried. After grit blasting, the average surface roughness was measured using the surface roughness tester (Make Mitutoyo, Japan; Model: Surftest 301). The average roughness was found to be ~ 5 µm.

2.4.2. Metallographic preparation

Metallographic cross sections of the coatings were prepared for the porosity and microhardness measurements. The samples were first carefully cut to the specific dimensions ($10 \times 10 \times 2$ mm^3). They were then mounted with low viscosity epoxy resin under vacuum environment. The mounted

Table 2
Important plasma spray parameters and their levels.

No	Factors	Notations	Units	Levels				
				-1.682	-1	0	1	1.682
1	Power	P	kW	20	21.62	24	26.38	28
2	Standoff distance	D	mm	100	106	115	124	130
3	Powder feed rate	F	g/min	18	22	28	34	38

Table 3
Design matrix and experimental results.

Expt. no.	Coded value			Original value			Response	
	Power (P)	Standoff distance (D)	Powder feed rate (F)	Power (kW)	Standoff distance (mm)	Powder feed rate (g/m)	Porosity (vol%)	Microhardness (HV)
1	-1	-1	-1	21.62	106	22	18	647
2	1	-1	-1	26.38	106	22	6	995
3	-1	1	-1	21.62	124	22	24	600
4	1	1	-1	26.38	124	22	9	987
5	-1	-1	1	21.62	106	34	18	802
6	1	-1	1	26.38	106	34	12	930
7	-1	1	1	21.62	124	34	28	537
8	1	1	1	26.38	124	34	20	701
9	-1.682	0	0	20	115	28	23	621
10	1.682	0	0	28	115	28	6	1034
11	0	-1.682	0	24	100	28	13	908
12	0	1.682	0	24	130	28	25	678
13	0	0	-1.682	24	115	18	10	867
14	0	0	1.682	24	115	34	18	721
15	0	0	0	24	115	28	5	1088
16	0	0	0	24	115	28	6	1069
17	0	0	0	24	115	28	5	1092
18	0	0	0	24	115	28	6	1088
19	0	0	0	24	115	28	5	1089
20	0	0	0	24	115	28	5	1088

samples were successively ground with 600, 800, 1000 and 1500 grit SiC papers and eventually polished using diamond slurries of 10–8, 8–5, 5–2, 2–0.5, 0.5–0 μm during 5, 5, 7, 10 and 10 min, respectively. Because of pullouts in brittle materials, it is difficult to establish and evaluate true porosity in a metallographically prepared spray coating. As metallographic grinding and polishing, if not carried out correctly, can introduce artifacts which are not part of the coating structure. Ceramic coatings are brittle and particles break out of the surface during grinding. If not polished thoroughly, these breakouts leave an incorrect impression of a high porosity. Similar procedures were followed by the other investigators [21,39,40].

2.4.3. Porosity analysis

Porosity measurement was carried out using an image analysis method [41] on the metallographic cross sections according to the ASTM B276 standard [42] on the polished cross-section of the coating, using an optical microscope (Make: Meiji; Japan, Model: MIL-7100) equipped with an image analyzing system (Metalvison version. 6). While carrying out image analysis, proper magnification has to be selected in order to reveal the features of images such as open pores and network of cracks. In this investigation, 400 × magnifications of optical micrographs with a image resolution of 1024×768 pixels were chosen for porosity analysis. Initially, a 200 μm square area was selected on the polished cross-section of the coating, and the image was analyzed. The same procedure was repeated at five random locations to find out the average percentage volume of porosity. Previous studies [10,25,43] show that depending on the purpose, comparisons are usually based on micrographs taken at magnifications ranging from 50 to 500 times. It is evident from the porosity analysis that images captured at 400 × magnification revealed the intricate features of plasma-sprayed coatings such as type A and type B pores. Costil et al. [44] also discussed about the resolution of images and predicted responses. They opined that image resolution has uncertainties such as high resolution leads to overvaluation in predicting values and hence the analyzed results have to be considered indicative rather than exact.

The steps involved in image analysis are shown in Fig. 4 and results show the presence type A and type B pores usually formed in plasma-sprayed coatings. Pore size and pores are classified from 0 to 10 μm as type A and designated as A02, A04, A06 and A08. Pores classification in the range from 10 to 25 μm as type B and designated as B02, B04, B06 and B08. Type A pores may be formed as a result of interaction between the material particles and the gaseous media. The type B pores are caused by the splashing of particles on impact with deposited material; or it may be due to voids resulting from the poor deformation of partially melted particles. These pores can have different sizes and exceedingly intricate shapes [42,45]. Moreover, results show that coating consists of type A and type B pores and distributed as A08 and B08 forms which are evidence of the characteristics of plasma-sprayed coating.

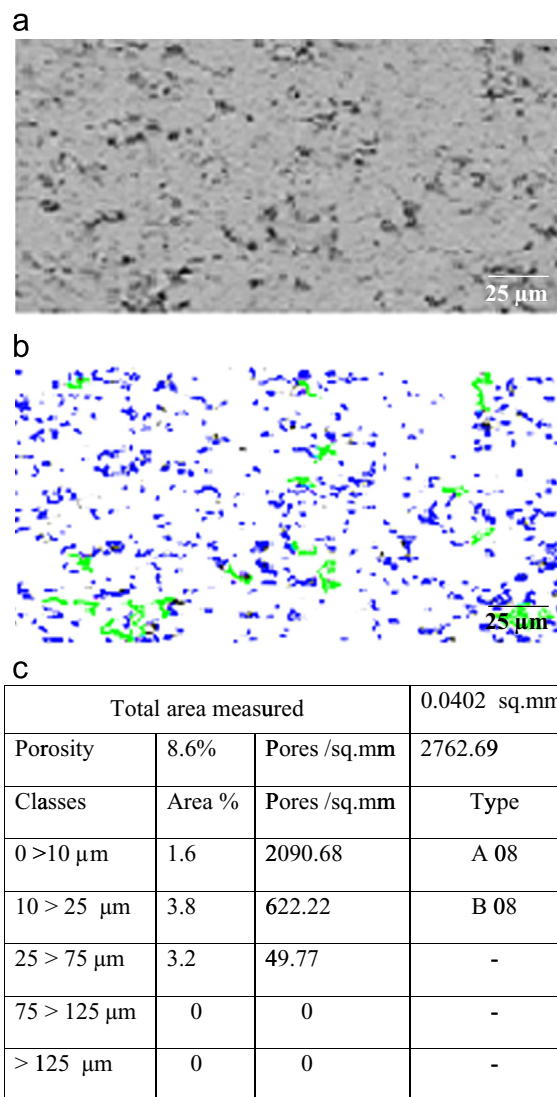| Total area measured			0.0402 sq.mm
Porosity	8.6%	Pores /sq.mm	2762.69
Classes	Area %	Pores /sq.mm	Type
0 >10 μm	1.6	2090.68	A 08
10 > 25 μm	3.8	622.22	B 08
25 > 75 μm	3.2	49.77	-
75 > 125 μm	0	0	-
> 125 μm	0	0	-

Fig. 4. Steps involved in coating porosity analysis and results of coating porosity analysis for Expt. no. 4. (a) Optical image selected for analysis, Expt. No. 4, (b) colour coded overlay image for pore identification and (c) results summary of porosity analysis.

2.4.4. Microhardness measurements

Microhardness measurements were operated by indenting on the metallographic cross sections under 300 g load for 15 s using a Vickers microhardness tester (Make: Shimadzu, Japan; Model: HMV-2T). For each coating sample, the measurement series comprised 20 random indentations. Distance between indentations was kept three times longer than the indentation diagonal to prevent the effects of the stress field of nearby indentations. Some of the indentation images on cross section of the coatings are shown in Fig. 5.

2.5. Developing empirical relationships

For prediction, response surface methodology (RSM) is practical, economical, and relatively easy for use [46]. Response surface methodology (RSM) is a collection of mathematical tool and statistical technique useful for analyzing problems in which several independent variables influence dependent variables or
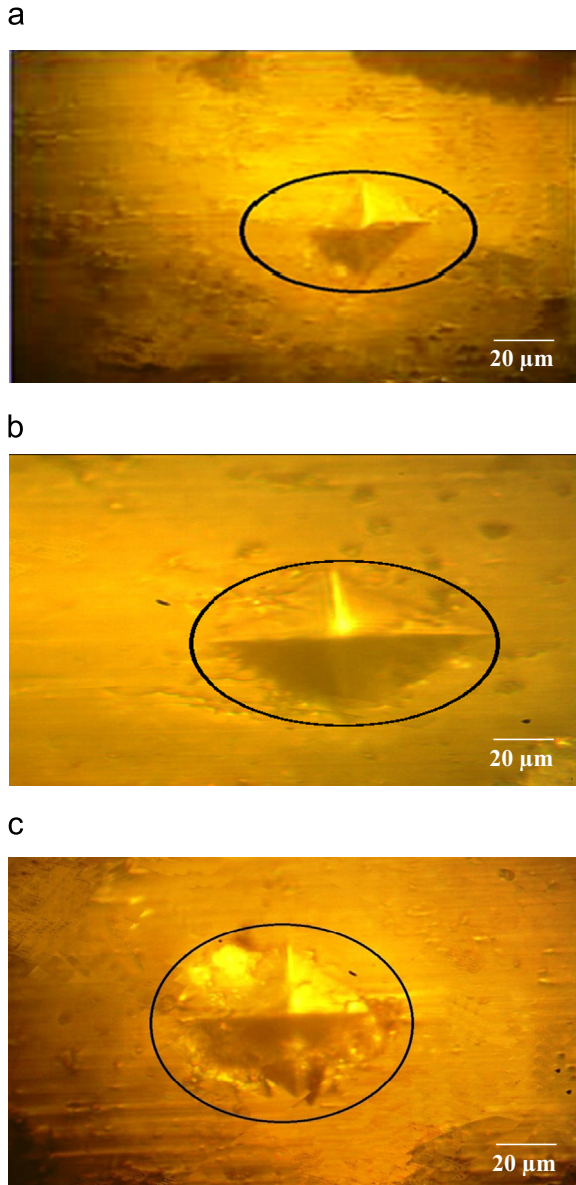
Fig. 5. Microhardness indentation images for various spray parameters. (a) Indentation image for spray expt. no. 2 shows no cracks at the indentation tips, (b) indentation image for spray expt. no. 6 shows no cracks at the indentation tips but forms at the sides and (c) indentation image for spray expt. no. 12 shows severe cracking at the indentation tips.

response and the goal is to optimize the response [47]. In applying the RSM, the independent variable was viewed as a surface to which a mathematical model is fitted. In order to correlate the process parameters and the responses of APS coating deposits, a second-order quadratic model [48] was developed to predict the responses based on the experimentally measured values. Porosity and microhardness are functions of the plasma spraying parameters such as input power (P), standoff distance (D) and powder feed rate (F), and it can be expressed as responses $= f(P, D, F)$.

The second-order polynomial (regression) equation is used to represent the response surface Y is given by

$$Y = \beta_0 + \sum \beta_i X_i + \sum \beta_{ii} X_i^2 + \sum \beta_{ij} X_i X_j \qquad (2)$$

The selected model should include the effects of main and interaction effects of all the factors. With the view of considering this criterion, for the three factors, the selected polynomial can be expressed as

$$
\begin{aligned}
Y = {} & b_0 + b_1(P) + b_2(D) + b_3(F) + b_{12}(PD) + b_{13}(PF) \\
& + b_{23}(DF) + b_{11}(P^2) + b_{22}(D^2) + b_{33}(F^2)
\end{aligned} \qquad (3)
$$

where b_0 is the average of the responses and $b_1, b_2, b_3, \ldots, b_{33}$ are regression coefficients that depend on respective linear, interaction, and squared terms of factors. In order to estimate the regression coefficients, a number of experimental design techniques are available. In this work, central composite rotatable design was used which fits the second-order response. All the coefficients were obtained applying central composite rotatable design using the Design-Expert statistical software package (Version 8.07.1). The significance of each coefficient was determined by Student's t test and p values, which are listed in Tables 4 and 5. In this case, P, D, F, PD, PF, DF, P^2, D^2 and F^2 are significant model terms, values of "Prob $> F$" less than 0.05 indicates that model terms are significant. After determining the significant coefficients (at 95% confidence level), the final empirical relationship was constructed using only these coefficients and the final mathematical model to estimate porosity and microhardness is given below:

$$
\begin{aligned}
\text{Porosity} = {} & (5.322629 - 4.9492P + 3.601233D + 2.253268F \\
& - 0.875PD + 1.875PF + 1.375DF + 3.310862996P^2 \\
& + 4.901853D^2 + 2.95731F^2)\ \text{vol\%}
\end{aligned} \qquad (4)
$$

$$
\begin{aligned}
\text{Micohardness} = {} & (1086.083932 + 126.0598P - 68.5233D \\
& - 36.9442F + 9.375PD - 55.375PF - 54.875DF \\
& - 94.00275057P^2 - 106.2003425D^2 \\
& - 105.847F^2)\ \text{HV}
\end{aligned} \qquad (5)
$$

2.6. Checking adequacy of the developed model

Analysis of variance (ANOVA) technique was used to check the adequacy of the developed empirical relationships. In this investigation, the desired level of confidence was considered to be 95%. The relationship may be considered to be adequate provided that

(a) the calculated value of the F ratio of the model developed should not exceed the standard tabulated value of F ratio and
(b) the calculated value of the R ratio of the developed relationship should exceed the standard tabulated value of R ratio for a desired level of confidence.

It is found that the model is adequate. The value of probability $> F$ in Tables 4 and 5 for the empirical relationships are less than 0.05, which indicates that the empirical relationships are significant. Lack of fit was not significant for all the developed empirical relationships as desired. Fisher's F test with a very low probability value (P model $> F = 0.0001$) demonstrates a very high significance. The goodness of fit of

Table 4
ANOVA test results for porosity.

Source	Sum of squares	Df	Mean square	F-value	p-value prob > F	
Model	1182.25	9	131.36	570.29	< 0.0001	Significant
P—power	344.49	1	344.49	1495.57	< 0.0001	
D—standoff distance	169.98	1	169.98	737.97	< 0.0001	
F—powder feed rate	81.95	1	81.95	355.78	< 0.0001	
PD	2.00	1	2.00	8.68	0.0146	
PF	18.00	1	18.00	78.15	< 0.0001	
DF	8.00	1	8.00	34.73	0.0002	
P^2	161.99	1	161.99	703.27	< 0.0001	
D^2	352.21	1	352.21	1529.09	< 0.0001	
F^2	145.36	1	145.36	631.06		
Residual	2.30	10	0.23			
Lack of fit	0.97	5	0.19	0.73	0.6322	Not significant
Pure error	1.33	5	0.27	570.29		
Cor total	1184.55	19	131.36	1495.57		
Std. dev	=0.48	R^2		= 0.9981	Df: degrees of freedom	
Mean	=13.15	Adjusted R^2		= 0.9963	CV: coefficient of variation	
CV%	=3.65	Predicted R^2		= 0.9922	F: Fisher ratio	
PRESS	=9.24	Adequate precision		= 66.218	p: probability	

Table 5
ANOVA test results for microhardness.

Source	Sum of squares	Df	Mean square	F-value	p-value prob > F	
Model	726,055	9	80,672.78	581.7321	< 0.0001	Significant
P—power	217,022.1	1	217,022.1	1564.948	< 0.0001	
D—standoff distance	64,124.93	1	64,124.93	462.4054	< 0.0001	
F—feed rate	18,639.9	1	18,639.9	134.4125	< 0.0001	
PD	703.125	1	703.125	5.070241	0.0480	
PF	24,531.13	1	24,531.13	176.8942	< 0.0001	
DF	24,090.13	1	24,090.13	173.7141	< 0.0001	
P^2	127,345.6	1	127,345.6	918.2904	< 0.0001	
D^2	162,537.9	1	162,537.9	1172.062	< 0.0001	
F^2	161,457.5	1	161,457.5	1164.272	< 0.0001	
Residual	1386.769	10	138.6769			
Lack of fit	1041.435	5	208.287	3.015739	0.1255	Not significant
Pure error	345.3333	5	69.06667			
Cor total	727,441.8	19				
Std. dev	11.77611	R^2		0.998094	Df: degrees of freedom	
Mean	877.1	Adjusted R^2		0.996378	CV: coefficient of variation	
CV%	1.342619	Predicted R^2		0.988475	F: Fisher ratio	
PRESS	8383.554	Adequate precision		65.62437	p: probability	

the model was checked by the determination coefficient (R^2). The coefficient of determination (R^2) was calculated to be 0.9981 for response. This implies that 99.81% of experimental data confirms the compatibility with the data predicted by the model, and the model does not explain only about 0.19% of the total variations. The R^2 value is always between 0 and 1, and its value indicates aptness of the model. For a good statistical model, R^2 value should be close to 1.0. The adjusted R^2 value reconstructs the expression with the significant terms. The value of the adjusted determination coefficient (adj R^2=0.9963) also high to advocate for a high significance of the model. The pred. R^2 (0.9922) that implies that the model could explain 95% of the variability in predicting new

observations. This is in reasonable agreement with the adj R^2 of porosity analysis. The value of coefficient of variation is also around 3.65 indicates that the deviations between experimental and predicted values are low. Adeq. precision measures the signal-to-noise ratio. A ratio greater than 4 is desirable. In this investigation, the ratio 66.218 which indicates an adequate signal. This model can be used to navigate the design space and able to predict the responses for a given input in the coded form. Similarly, the ANOVA analysis of microhardness is presented in Table 5. From the table, it is understood that the developed statistical model was found be adequate at 95% confidence level. Coefficient of determination 'R^2' was used to find how close the predicted and experimental values lie. The
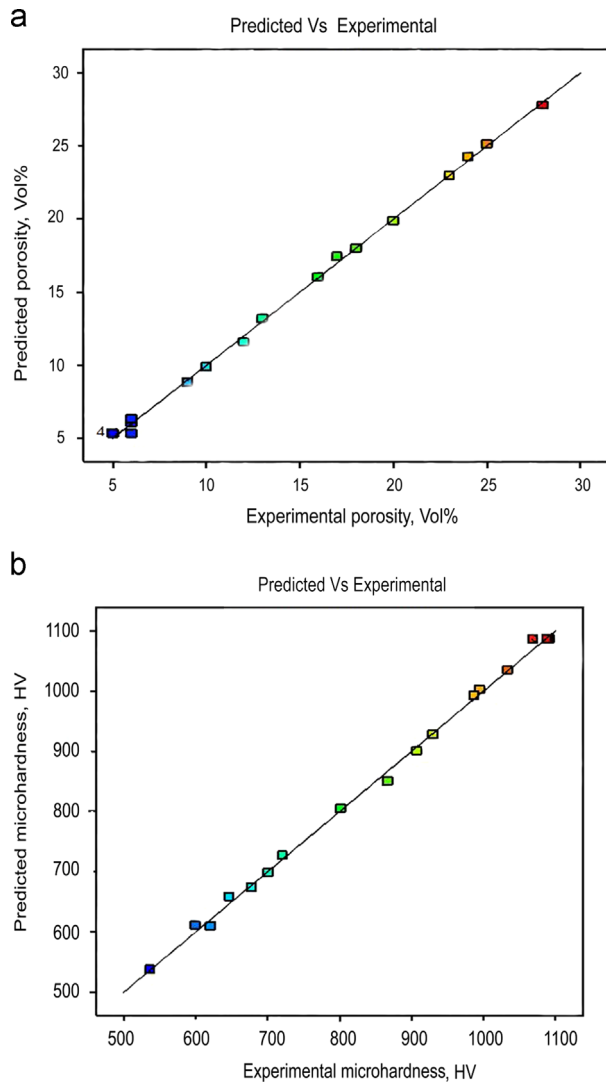
a

b

a

b

Fig. 6. Experimental values vs. predicted values. (a) Correlation graph for porosity and (b) correlation graph for microhardness.
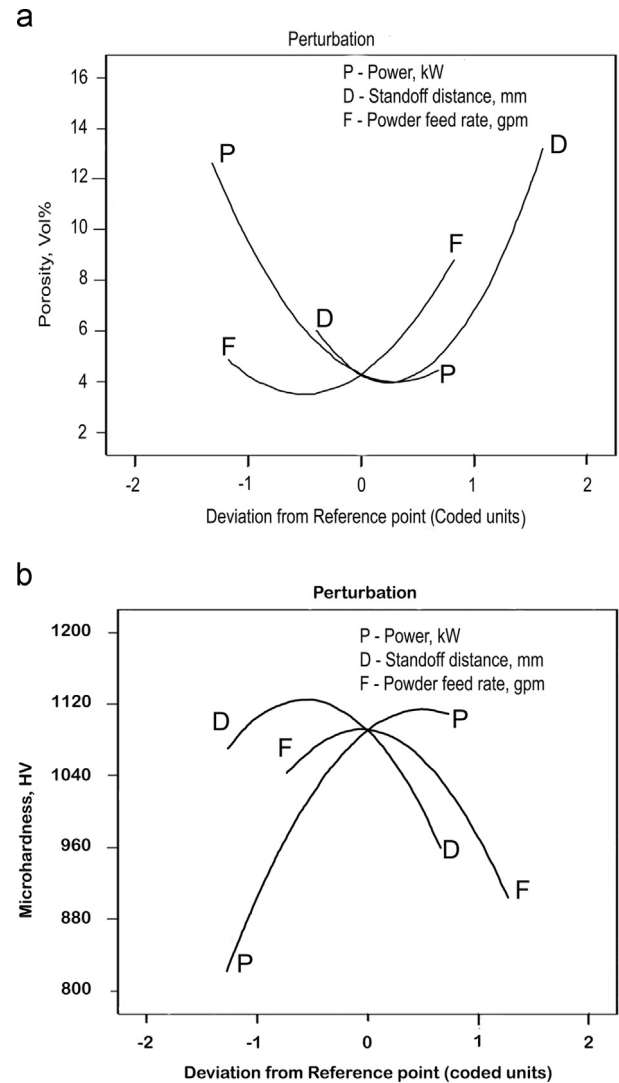
Fig. 7. Perturbation plots shows the dependence of spray parameters on coating characteristics. (a) Effect of plasma spray parameters on porosity and (b) effect of plasma spray parameters on microhardness.

value of 'R^2' for the above-developed model was calculated and is presented in Table 5, which indicates that a high correlation exists between estimated values and experimental values. Further, correlation graphs were drawn relating experimental values and predicted values as shown in Fig. 6 and it is found that the developed empirical relationships can be effectively used for prediction purpose.

3. Results and discussion

3.1. Perturbation plots

The developed empirical relationships can be used effectively to predict the responses by substituting process parameter values in the coded form. Based on these empirical relationships, the main and interaction effects of the process parameters on the coating properties were computed and plotted in the form of perturbation plots, as shown in Fig. 7. The perturbation plot is an important diagrammatic representation, which provides silhouette views of the response surface

[49]. The perturbation plot can be used to compare the effects of all factors at a specific point in the RSM design space. For response surface designs, the perturbation plot shows how the response changes as each factor moves from the selected reference point, while all other factors remain constant at the reference value. Normally, Design-Expert software sets the reference point default at the middle of the design space (the coded zero level of each factor). A steep slope or curve in a factor shows that the response is sensitive in that factor. A relatively flat line shows insensitivity to change in that particular factor [50].

Further, using the F values, the predominant factors, which have the major and minor effects on the responses could be assessed. From the F-value assessment, it was found that the predominant factors which have direct influence on the responses as per hierarchy are power, standoff distance and powder feed rate. This pronounced effect also has been observed from Fig. 7 and shows good agreement with the predicted model F values.

3.2. Dependence of porosity and microhardness on spray parameters

Fig. 7(a and b) shows the perturbation plots which are drawn from the results calculated by the regression Eqs. (4) and (5). From the experimental results, it is observed that within the range of experimental design space, the higher the input power, the lower is the porosity. It is well known that during plasma spraying, an electric arc is initiated between the two electrodes using a high frequency discharge and then sustained using power. The arc ionizes the gas, creating high-pressure gas plasma which contains higher heat content. The resulting increase in gas temperature, which may exceed 30,000 °C, in turn increases the volume of the gas. Increasing the power level, increases the enthalpy in the plasma flame, is likely to melt the particles, which in turn increases particle-melting ratio subsequently enhances good compaction of the coating obtained during coating buildup. Further, effective flattening and solidification of the particles over the deposited layers will lead to reduce the porosity and increasing microhardness values [51].

When increasing standoff distance, the molten particles in the plume loses its enthalpy largely, this leads to decelerate the inflight particle velocity, particles striking on the substrate will experience poor flattening over the previously deposited layers, resulting in increased porosity and reduced microhardness values. At smaller standoff distance, possibility of splashing of molten particles and quench cracks end up with increased level of porosity [52]. Standoff distance is of substantial importance because adequate distance must be provided for heating and accelerating the powder, but too great a distance will allow the powder to cool and lose velocity, because the gas stream which is rapidly expanding, cooling, and slowing will end up with molten droplets that land on substrate without enough kinetic energy to form splats. These droplets can stay on the substrate by themselves [53] and leads to increased coating roughness which resulted in lower microhardness.

Powder is usually introduced into the plasma plume either just outside the torch or in the diverging exit region of the nozzle (anode). It is both heated and accelerated by the high-temperature, high-velocity plasma gas stream. The variations in powder feed rate on the coating characteristics are displayed in Fig. 7. It is well known that the increasing the powder feed rate in the plasma plume will reduce the enthalpy transfer to the injected particles. This will affect the inflight particles melting state and velocity. Moreover, particle temperature and velocity strongly influence the splat formation during coating buildup. It is important to use the thermal energy stored in the plasma effectively, inflight processing should be performed under high loading conditions [54]. When lower amount of powder has been supplied to the flame that will end up with vaporization and/or over melting of the particles resulting in higher porosity and lowering microhardness. Higher feed rates will lead to even lower plasma temperatures [55] resulting in poor melting of the powder particles resulting in a decrease of the splat flattening ratio and an increase in the porosity.
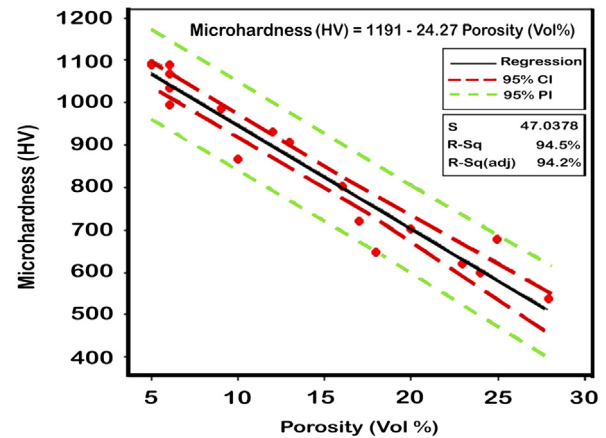

Fig. 8. Relationship graph for porosity and microhardness.

Considering individual process parameter, it is very clear that the porosity of the coating is not much sensitive to the powder feed rate. The same trend can be observed in the model 'F' values (355.78) and good agreement was found.

3.3. Relationship between porosity and microhardness of YSZ coatings

The coating porosity and the coating microhardness obtained from the experimental results are related as shown in Fig. 8. The experimental data points are fitted by a straight line. The straight line is governed by the following regression equation:

$$\text{Microhardness (HV)} = 1191 - 24.27 \ (\text{porosity in vol\%}) \qquad (6)$$

The slope of the estimated regression equation (-24.27) is negative, implying that as porosity decreases, microhardness increases. The coefficient of determination is $R^2 = 94.5\%$. It can be interpreted as the percentage of the total sum of squares that can be explained by using the estimated regression equation. The coefficient of determination R^2 is a measure of the goodness of fit of the estimated regression equation [56]. The fitted regression line (Eq. (6)) may be used for two purposes:

(a) To estimate the mean value of coating microhardness for the given value of coating porosity.
(b) Predicting an individual value of coating microhardness for a given value of coating porosity level.

The confidence interval and prediction interval show the precision of the regression results. Narrower intervals provide a higher degree of precision (Fig. 8). Confidence interval (CI) is an interval estimate of the mean value of y for a given value of x. Prediction interval (PI) is an interval estimate of an individual value of y for a given value of x. The estimated regression equation provides a point estimate of the mean value of microhardness for a given value of porosity. The difference between CI and PI reflects the fact that it is possible

to estimate the mean value of microhardness more precisely than an individual value of microhardness. The greater width of the PI is reflecting the added variability introduced by predicting a value of the random variable as opposed to estimating a mean value. From Fig. 8, it is also inferred that the closer the value to 'X' (15.21 vol%) the narrower will be the interval.

3.4. Developing process maps for coating design and tailoring coating properties

Perturbation plots provide the sensitiveness of the spray parameters and compare the results of values deduced from the regression equations. This perturbation plots offer a relationship for a given input power/standoff distance/powder feed rate to the coating characteristics. These plots are very useful to identify important parameter, track instabilities and examine reliability of process. However, to utilize such plots from a coating design and microstructural tailoring perspective, it is important to combine coating properties with the spray parameters. Selection of input variables for achieving the required qualities of coating is the main problem faced in the manufacture of yttria-stabilized zirconia coatings by the atmospheric plasma spraying process. This problem can be solved by the identification of relationships between the process parameters (input power, standoff distance and powder feed rate) and the coating quality characteristics.

On the basis of coating properties determined from the regression equations, characteristic regimes of properties can be identified and overlaid on the graph are displayed in Fig. 9. Two different property contours superimposed on plot to identify appropriate regime which can be used for tailoring coating properties. Zone-I, zone-II and zone-III represent three regimes of coating properties and their relationships to spray conditions. Such a plot provides a chance to optimize coating microstructure based on multifunctional design requirements. The zones represented in the figures can be broadly described as follows:

(a) Zone-I: low porosity and higher microhardness regime.
(b) Zone-II: low porosity and moderate microhardness regime.
(c) Zone-III: higher porosity and moderate microhardness regime.

It is notable that the locations of zones I and II provide lower porosity and higher microhardness when compared with zone-III. Although it is noticed that the microhardness data in Fig. 9b do not follow the well known trend of higher stiffness with the increased kinetic energy of the particles. The results obtained from the zone maps are consistent with the experimental results shown earlier, in that coating no. 2 shows the greatest stiffness and higher hardness while coating no.12 displays a higher porosity and lower hardness associated with a low modulus [57]. The process map establishes the connection between spray parameters and property relations to attain mechanical compliance of TBC coatings and as such offers a unique approach to tailoring coating properties. A high amount
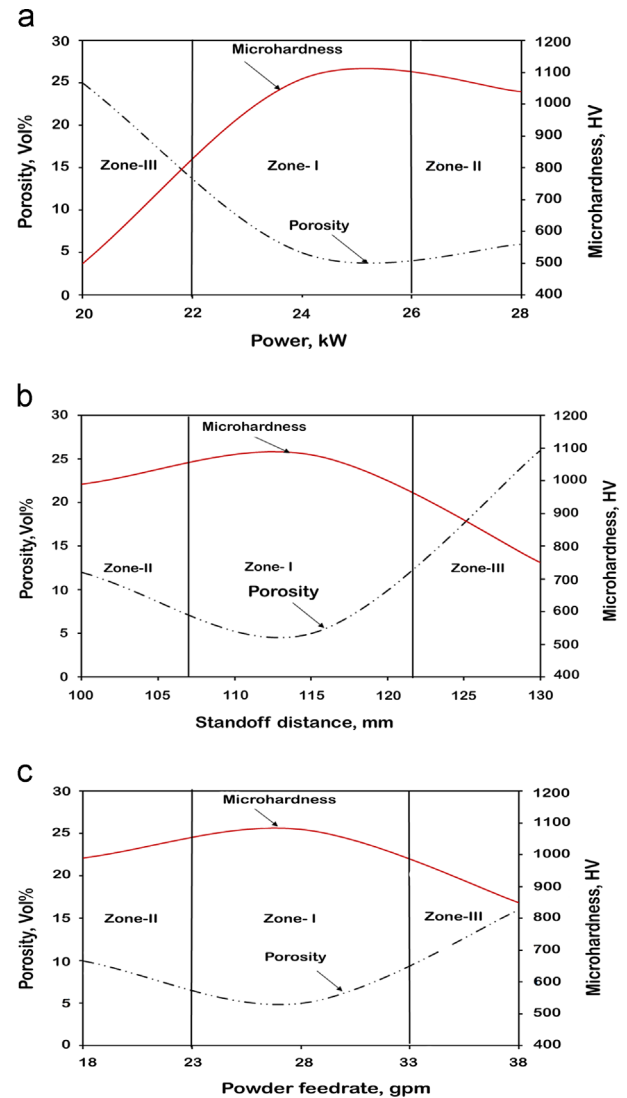

Fig. 9. Process maps to tailor coating characteristics. (a) Effect of input power, (b) effect of standoff distance and (c) effect of powder feed rate.

of porosity would involve very quick oxygen ingress to the bond coat and results in a failure by oxidation. However, too low a porosity level, on the other hand, reduces the ability of the coatings to accommodate stress. Therefore, a critical amount of porosity in the ceramic overlays must be achieved [58]. The selection of zone-III was based on the desired characteristics for TBC applications, such as low thermal conductivity and high compliance.

From these superimposed contour maps, a specific process zone can be identified representing a desired combination of the above three properties. Since the spray parameters and coating characteristic properties are linked it is now feasible to access a specific property regime via process control in a fully integrated scheme represented by zone-I, zone-II and zone-III in the figure.

4. Conclusions

1. Empirical relationships were developed to predict (at 95% confidence level) the porosity and microhardness of yttria-

stabilized zirconia coatings incorporating predominant plasma spray parameters such as input power, standoff distance and powder feed rate.

2. Of the three plasma spray parameters studied in this investigation, input power has the largest effect on the coating characteristics followed by standoff distance and powder feed rate.

3. A regression equation has been developed incorporating coating porosity and microhardness of the coating. This equation can be effectively used to predict microhardness of YSZ coating, if coating porosity is known.

4. With the help of integrated spray parameters and coating characteristics process maps, a specific process zone can be identified representing a desired combination for the specific applications.

Acknowledgments

References

[1] N.P. Padture, M. Gell, E.H. Jordan, Thermal barrier coatings for gas turbine engine applications, Science 296 (2002) 280–284.

[2] H.B. Guo, R. Vaßen, D. Stover, Thermophysical properties and thermal cycling behavior of plasma sprayed thick thermal barrier coatings, Surf. Coat. Technol. 192 (2005) 48–56.

[3] R.A. Miller, Thermal barrier coatings for aircraft engines: history and directions, J. Therm. Spray Technol. 6 (1997) 35–42.

[4] N.P. Padture, K.W. Schlichting, T. Bhatia, A. Ozturk, B. Cetegen, E.H. Jordan, M. Gell, S. Jiang, T.D. Xiao, P.R. Strutt, E. Garcia, P. Miranzo, M.I. Osendi, Towards durable thermal barrier coatings with novel microstructures deposited by solution precursor plasma spray, Acta Mater. 49 (2001) 2251–2257.

[5] A. Vaidya, V. Srinivasan, T. Streibl, M. Friis, W. Chi, S. Sampath, Process maps for plasma spraying of yttria-stabilized zirconia: an integrated approach to design, optimization and reliability, Mater. Sci. Eng., A 497 (2008) 239–253.

[6] T.A. Choudhury, N. Hosseinzadeh, C.C. Berndt, Artificial neural network application for predicting in-flight particle characteristics of an atmospheric plasma spray process, Surf. Coat. Technol. 205 (2011) 4886–4895.

[7] P. Fauchais, M. Vardelle, A. Vardelle, L. Bianchi, Plasma spray: study of the coating generation, Ceram. Int. 22 (1996) 295–303.

[8] D. Schwingel, R. Taylor, T. Haubold, J. Wigren, C. Gualco, Mechanical and thermophysical properties of thick PYSZ thermal barrier coatings correlation with microstructure and spraying parameters, Surf. Coat. Technol. 108 (1998) 99–106.

[9] Q.I. Hong Yu, Zhou Lr Zhu, Yang Xiao Guang, Measurement of Young's modulus and Poisson's ratio of thermal barrier coatings, Chi. J. Aeronaut. 18 (2005) 180–184.

[10] C.J. Li, A. Ohmori, Relationship between the microstructure and properties of thermally sprayed deposits, J. Therm. Spray Technol. 11 (3) (2002) 365–374.

[11] H. Herman, N.R. Shankar, Survivability of thermal barrier coatings, Mater. Sci. Eng. A 88 (1987) 69–74.

[12] R. Vassen, F. Traeger, D. Stover, Correlation between spraying conditions and microcrack density and their influence on thermal cycling life of thermal barrier coatings, J. Therm. Spray Technol. 13 (3) (2004) 396–404.

[13] B.Z. Janos, E. Lugscheider, P. Remer, Effect of thermal aging on the erosion resistance of air plasma sprayed zirconia thermal barrier coatings, Surf. Coat. Technol. 113 (1999) 278–285.

[14] N.A. Jarrah, Studying the influence of process parameters on the catalytic carbon nano fibers formation using factorial design, J. Chem. Eng. 151 (2009) 367–371.

[15] C. Pierlot, L. Pawlowski, M Bigan, P. Chagnon, Design of experiments in thermal spraying: a review, Surf. Coat. Technol. 202 (2008) 4483–4490.

[16] T. Troczynski, M. Plamondon, Response surface methodology for optimization of plasma spraying, J. Therm. Spray Technol. 1 (1992) 293–300.

[17] T. Valente, Statistical evaluation of Vicker's indentation test results for thermally sprayed materials, Surf. Coat. Technol. 90 (1997) 14–20.

[18] D.J. Varacalle Jr, L.B. Lundberg, H. Herman, G. Bancke, W.L. Riggs II, Vacuum plasma sprayed zirconium carbide coatings, Surf. Coat. Technol. 68 (1994) 86–91.

[19] S. Dyshlovenko, L. Pawlowski, P. Roussel, D. Murano, A. Le Maguer, Relationship between plasma spray operational parameters and microstructure of hydroxyapatite coatings and powder sprayed into water, Surf. Coat. Technol. 200 (2006) 3845–3855.

[20] J.R. Mawdsley, Y.J. Su, K.T. Faber, T.F. Bernecki, Optimization of small-particle plasma-sprayed alumina coatings using designed experiments, Mater. Sci. Eng. A 308 (2001) 189–199.

[21] J.F. Li, H. Liao, B. Normand, C. Cordier, G. Maurin, J. Foct, C. Coddet, Uniform design method for optimization of process parameters of plasma sprayed TiN coatings, Surf. Coat. Technol. 176 (2003) 1–13.

[22] J.F. Li, H.L. Liao, C.X. Ding, C. Coddet, Optimizing the plasma spray process parameters of yttria stabilized zirconia coatings using a uniform design of experiments, J. Mater. Proc. Technol. 160 (2005) 34–42.

[23] F. Azarmi, T.W. Coyle, J. Mostaghimi, Optimization of atmospheric plasma spray process parameters using a design of experiment for alloy 625 coating, J. Therm. Spray Technol. 17 (1) (2008) 144–155.

[24] S.M. Forghani, M.J. Ghazali, A. Muchtar, A.R. Daud, N.H.N. Yusoff, C.H. Azhari, Effects of plasma spray parameters on TiO_2-coated mild steel using design of experiment (DoE) approach, Ceram. Int. 39 (2013) 3121–3127.

[25] R.B. Hiemann, Plasma-Spray Coating-Principles and Applications, Wiley VCH Publishers Inc, New York, 1996.

[26] R. Suryanarayanan, Plasma Spraying: Theory and Applications, World Scientific Publishing, New York, 1993.

[27] L. Pawlowski, The Science Engineering of Thermal Spray Coatings, second ed., John Wiley & Sons Ltd, London, 2008.

[28] C.S. Ramachandran, V. Balasubramanian, P.V. Ananthapadmanabhan, Multi objective optimization of atmospheric plasma spray process parameters to deposit yttria-stabilized zirconia coatings using response surface methodology, J. Therm. Spray Technol. 20 (3) (2011) 590–608.

[29] D. Thirumalaikumarasamy, K. Shanmugam, V. Balasubramanian, Influences of atmospheric plasma spraying parameters on the porosity level of alumina coating on AZ31B magnesium alloy using response surface methodology, Prog. Nat. Sci.: Mater. Int. 22 (5) (2012) 468–479.

[30] S. Kuroda, T.W. Clyne, The quenching stress in thermally sprayed coatings, Thin Solid Films 200 (1991) 49–66.

[31] Kuroda, T. Dendo, S. Kitahara, Quenching stress in plasma sprayed coatings and its correlation with the deposit microstructure, J. Therm. Spray Technol. 4 (1995) 75–84.

[32] V. Srinivasan, M. Friis, A. Vaidya, T. Streibl, S. Sampath, Particle injection in direct current air plasma spray: salient observations and optimization strategies, Plasma Chem. Plasma Process. 27 (2007) 609–623.

[33] Scrivani Andrea, Gabriele Rizzi, Christoper C. Berndt, Enhanced thick thermal barrier coatings that exhibit varying porosity, Mater. Sci. Eng. A 476 (2008) 1–7.

[34] R. Ramasamy, V. Selvarajan, K. Perumal, G. Shanmugavelayutham, An attempt to develop relations for the arc voltage in relation to the arc current and gas, Vacuum 59 (2000) 118–125.

[35] A.I. Khuri, J.A. Cornell, Response Surfaces: Design and Analysis, Marcel Dekker Ltd, New York, 1996.

[36] W.G. Cochran, G.M. Cox, Experimental Designs, second ed., John Wiley &Sons (Asia) Pte Ltd, Singapore, 1992.

[37] R.G. Miller, J.E. Freund, D.E. Johnson, Probability and Statistics for Engineers, Prentice Hall of India Pvt. Ltd, New Delhi, 1999.

[38] D.C. Montgomery, Design and Analysis of Experiments, John Wiley & Sons Ltd, New Delhi, 2007.

[39] Robert C. Tucker, Jr., Thermal Spray Coatings, in: ASM Handbook, vol. 5. Surface Engineering, pp. 497–509.

[40] Metallographic Preparation of Thermal Spray Coatings, Application Notes from ⟨www.struers.com⟩.

[41] Hao Du, Jae Heyg Shin, Soo Wohn Lee, Study on porosity of plasma-sprayed coatings by digital image analysis method, J. Therm. Spray Technol. 14 (4) (2005) 453–461.

[42] ASTM B 276-05, Standard Test Method for Apparent Porosity in Cemented Carbides, American Society for Testing and Materials, Pennsylvania, 2010.

[43] G. Moskal, The porosity assessment of thermal barrier coatings obtained by APS method, J. Achiev. Mater. Manuf. Eng. 20 (1) (2007) 483–486.

[44] S. Costil, C. Verdy, R. Bolot, C. Codet, On the role of spraying process on microstructural, mechanical and thermal response of alumina coatings, in: B.R. Marple, M.M. Hyland, Y.C. Lau, C.J. Li, R.S. Lima, G. Montavon (Eds.), Thermal Spray 2007; Global Coating Solutions. ASM International, Materials Park, OH, USA, pp. 533–537, Copy right, 2007.

[45] G. Antou, R. Hlawska, R. Bolot, G. Montavon, C. Codet, A. Cornet, Pore network architecture and thermal conductivity of Y-PSZ TBCs in situ melting during their deposition, in: E. Lugscheider (Ed.), Proceedings of the ITSC Conference, Thermal Spray Connects: Explore Its Surface Potential, ASM International, Materials Park, OH, USA, 2005.

[46] S. Rajakumar, C. Muralidharan, V. Balasubramanian, Statistical analysis to predict grain size and hardness of the weld nugget of friction-stir-welded AA6061-T6 aluminium alloy joints, Int. J. Adv. Manuf. Technol. 57 (2011) 151–165.

[47] R. Karthikeyan, V. Balasubramanian, Predictions of the optimized friction stir spot welding process parameters for joining AA2024 aluminum alloy using RSM, Int. J. Adv. Manuf. Technol. 51 (2010) 173–183.

[48] V. Balasubramanian, A.K. Lakshminarayanan, R. Varahamoorthy, S. Babu, Understanding the parameters controlling plasma transferred arc hardfacing using response surface methodology, Mater. Manuf. Process. 23 (2008) 674–682.

[49] C.S. Ramachandran, V. Balasubramanian, P.V. Ananthapadmanabhan, V. Viswabaskaran, Understanding the dry sliding wear behaviour of atmospheric plasma sprayed rare earth oxide coatings, Mater. Des. 39 (2012) 234–252.

[50] R.H. Myers, D.C. Montgomery, Response Surface Methodology, John Wiley & Sons, Inc., New York, 2002.

[51] G. Montavon, C.C. Berndt, C. Coddet, S. Sampath, Herman, Quality control of the intrinsic deposition efficiency from the controls of the splat morphologies and the deposit microstructure, J. Therm. Spray Technol. 6 (1997) 153–166.

[52] A. Kucuk, C.C. Berndt, U. Senturk, R.S Lima, C.R.C. Lima, Influence of plasma spray parameters on mechanical properties of yttria stabilized zirconia coatings, i: four point bend test, Mater. Sci. Eng. A 284 (2000) 29–40.

[53] C.S. Ramachandran, V. Balasubramanian, P.V. Ananthapadmanabhan, On resultant properties of atmospheric plasma sprayed yttria stabilised zirconia coating deposits: designed experimental and characterization analysis, Surf. Eng. 27 (2011) 217–229.

[54] P. Fauchais, Understanding plasma spraying, J. Phys. D: Appl. Phys. 37 (2004) 86–108.

[55] R.L. Williamson, J.R. Fincke, C.H. Chang, A computational examination of the sources of statistical variance in particle parameters during thermal plasma spraying, Plasma Chem. Plasma Process. 20 (2000) 299–324.

[56] S. Rajakumar, C. Muralidharan, V Balasubramanian, Developing empirical relationships to predict grain size and hardness of the weld nugget of friction stir welded AA7075-T6 aluminium alloy joints, Exp. Tech. 36 (2012) 6–17.

[57] S. Karthikeyan, V. Balasubramanian, R. Rajendran, Application of response surface methodology to predict porosity and Young's modulus of plasma sprayed yttria stabilized zirconia coating for tbc applications, in: Proceedings of the Heat Treatment and Surface Engineering (ASM), Chennai, May 2013, OP 32.

[58] S. Das, P.P. Bandyopadhyay, S. Ghosh, T.K. Bandyopadhyay, A.B. Chattopadhyay, Processing and characterization of plasma-sprayed ceramic coatings on steel substrate. Part II: on coating performance, Metall. Mater. Trans. A 34A (2003) 1919–1930.